Research Article

Performance Enhancements of Fully Inkjet-Printing Technology for Antenna-in-Package and Substrate Integrated Waveguides

Yen-Sheng Chen and Sheng-Xue Huang

Department of Electronic Engineering, National Taipei University of Technology, Taipei, Taiwan

Correspondence should be addressed to Yen-Sheng Chen; yschen@ntut.edu.tw

A fully inkjet-printing technology is applied to antenna-in-package (AiP) and substrate integrated waveguide (SIW) to enhance the performance of three components, including via holes, wire bonding, and flexible antenna arrays. First of all, earlier studies utilize shorting pins for the conductive pathway in high-density AiP and SIW, but this requires an additional procedure to plate the conductor. We propose a mechanical approach to form a cylindrical hole, plating the surface with silver nanoparticles and realizing the equivalent circuit model of the shorting pin. The proposed approach does not require high alignment sensitivity or the precise control of laser power level. Second, fully inkjet-printed wire bonding is proposed for the system on the package. The proposed technique not only reduces the discontinuity but also enables a fabrication without additional assembly. Third, the proposed technique is implemented for antenna development, which shows desirable performance with reduced fabrication complexity. The proposed technology is validated by microstrip lines, SIWs, SIW cavity slots, and flexible 4×4 patch arrays fabricated on various substrates including RO 4003C, polyimide, and polyethylene naphthalate. For comparison purposes, conventional approaches using printed circuit boards are also implemented and tested. The results indicate the generality and capability of the proposed technique.

1. Introduction

Additive manufacturing (AM) is an emerging technology for fabricating electromagnetic (EM) passive circuits and antennas [1]. The additive process includes three-dimensional (3D) printing and two-dimensional (2D) inkjet printing. Among them, 3D printing shows the potential for facilitating spatial complex design [2], whereas inkjet-printing advances conventional printed circuit boards (PCBs) due to the direct-write feature, low fabrication cost, and the application of flexible, light, or environmental friendly substrates. Inkjet printing has served a wide range of EM applications, including antenna-in-package (AiP) applications [3], substrate integrated waveguide (SIW) circuits and antennas [4–6], flexible antennas [7–24] including origami [7–11] and wearable applications [12, 17, 21, 24], radiofrequency

identification (RFID) tags [25] and the chipless counterpart [26], and wireless sensors [27].

In particular, AiP and SIW applications rise to the challenge of three limitations. First of all, AiP and SIWs are constructed by numerous vias. The conventional fabrication process of the vias consists of drilling and plating, which requires conductive pins to be inserted into and soldered [28, 29]. Such an additional procedure is not compatible with inkjet printing, thereby decreasing the efficiency of manufacturing. Recent research has presented fully inkjet-printed vias that replace additional conductive pins [30, 31]. The drilling is based on the PCB microvia technique, namely, CO_2 laser drilling, whereas the topology of the via is stepped hole. The stepped via is expected to create a continuous transition and reduce the stress on silver nanoparticles. Nevertheless, shaping the stepped hole topology requires

flipping the substrate and drilling both sides with the precise control of the laser power level, which increases the difficulty of alignment. As such microvia fabrication aims at high-density PCB design, aligning a large number of via holes with zero tolerance for errors increases the cost and complexity.

Second, in AiP and system on package (SoP) applications, interconnection using wire bonding is widely used, whereas the performance is significantly influenced by the discontinuity introduced. A method to reduce the discontinuity is to print the bond wire along with the circuitry and antenna [19, 32]. As the overall structure is manufactured in a fully inkjet-printing manner, the AiP application can prevent additional assembly and discontinuity. However, the development of this approach has not been given the attention it needs.

The third challenge is the development of flexible antenna arrays. Previously, several flexible substrates have been implemented, including paper [7–11], polyethylene terephthalate (PET) [12–14], polyimide (PI) [15–17], liquid crystal polymer (LCP) [18], FLGR02 [19], polydimethylsiloxane (PDMS) [20], polytetrafluoroethylene (PTFE) [21], and leather [22]. The antenna configuration includes monopole [8–15], patch [14, 18, 20, 21], dipole [15], inverted-F [16], quasi-Yagi [19], and slot [22]. Most of the antenna is a single element [7–13, 15–17, 19–22]; however, relatively few studies propose inkjet-printed flexible antenna arrays [14, 18, 33–35]; and these antenna arrays have not been tested over folding angles. When multiple elements are excited as an array, flexible substrates rise to the challenge of a bending feeding network and the distortion of patterns. The direction of the main beam and nulls could be adversely affected. In addition, the impedance matching could be detuned. Thus, designing a flexible array structure is more challenging than developing a single element. More studies should be conducted to investigate the array structure on a flexible substrate.

The goal of this paper is to address the three limitations, enabling a low-cost, low-complexity, and fully inkjet-printing scheme for AiP, SIW, SoP, and flexible antenna arrays. We first demonstrate a via fabrication method for AiP and SIWs. The proposed technique conducts drilling by a mechanical approach without flipping a substrate, thereby removing the alignment error. The mechanical drilling also prevents the precise control of laser power levels. Furthermore, by printing a cylindrical-surface hole six times, silver nanoparticles can make a continuous pathway for each end. The proposed technique is validated in terms of two-port microstrip lines and SIWs fabricated on various substrates. The comparison between the proposed technique and the conventional shorting pin will be demonstrated. Next, the fully inkjet-printing mechanism is extended to wire bonding. The capability of the proposed technique will be exhibited through the test of continuity. Afterward, the fully inkjet-printing technique is applied to SIW cavity slot antennas and flexible 4×4 patch arrays. Simulated and measured results will be provided.

2. Fully Inkjet-Printed Via Hole with Reduced Fabrication Complexity

2.1. Proposed Via Hole.
The proposed fully inkjet-printed SIW reduces the misalignment mismatch, mechanical stress, and fabrication complexity from the conventional technique using laser driller. For thick substrates, the stepped-hole method drills the top side of the substrate and generates several concentric circular cylinders. The same procedure is performed for the bottom side of the substrate until each end is connected by the stepped hole, where the first and second steps of the top and bottom sides are drilled with the same radius, respectively. Thus, the alignment of the holes on each side requires high sensitivity. In addition, repetitive drilling may incur a larger amount of mechanical stress.

In contrast, the proposed method performs drilling using a mechanical approach, as shown in Figure 1. The positions of via are marked, and the through holes are generated for all the vias without flipping the substrate. The alignment issue is thus prevented. Moreover, as the process requires no repetitive drilling, the mechanical stress is reduced. The thermal stress is also lowered, for the through holes are drilled at a room temperature. Afterward, this cylindrical surface is plated with silver nanoparticles six times. The printing procedure employs a materials printer Fujifilm Dimatix DMP-2850 from SIGMA Technology, Taiwan, to deposit silver nanoparticles, the conductivity of which is 9.1×10^{6} S/m. The via holes are plated along with other conductive components; therefore, the generation of the overall structure is efficient. Although numerous via holes are present, plating the overall structure takes only 150 seconds. The material printer deposits nanoparticles to the drilling hole with a voltage of 30 V at 28°C. The gravity force stretches the inks along the cylindrical surface. While coating the surface for one time may result in discontinuity or cracks, printing the surface six times averages out the adverse effects, which further result in a continuous metallic pathway. After one set of the metallization process is completed, the inkjet-printed application is sintered from 40°C to 200°C, with an incremental step of 20°C. The final thickness of the conductor is 15 μm. Even though the surface is not drilled by the stepped topology, continuous and smooth conductive paths can be observed. The equivalent resistance of the via hole is about 1.0 mΩ.

2.2. Validation.
The proposed technique is suitable for various substrates with different thicknesses. For validation purposes, we test the conductive pathway and compare the performance with the conventional shorting pin. Figure 2 shows a microstrip line fabricated on multiple layers. The two substrates are RO 4003C (dielectric constant $\varepsilon_r = 3.55$ and loss tangent $\tan\delta = 0.0027$) with the same thickness of 0.813 mm. The design frequency is 2.4 GHz. The trace is implemented on the top substrate, but the middle segment is truncated purposely and embedded into the middle layer. The top and middle traces are interconnected by either the proposed via hole or the shorting pin, resulting in two test pieces for comparison. In addition, to evaluate the additional loss caused by the discontinuity, another test piece with a full trace on the upper layer is fabricated. The two-port scattering parameters of the three circuits are measured.

Figure 3 shows the simulated and measured results for the three microstrip lines. All circuits depict comparable
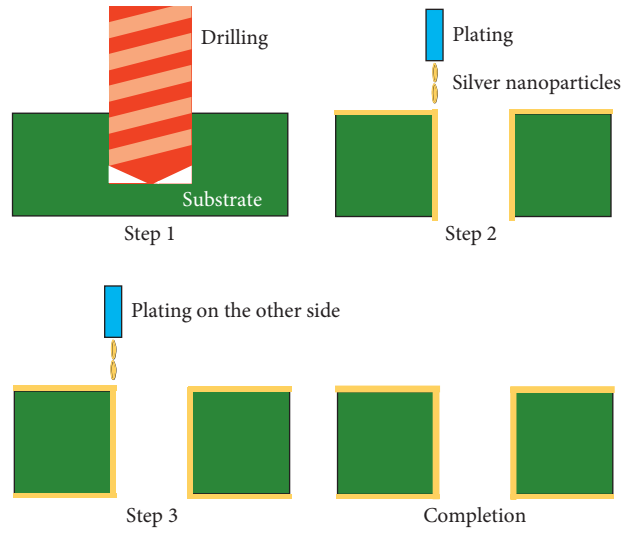
FIGURE 1: Fabrication process of the fully inkjet-printed via hole.

(a)   (b)
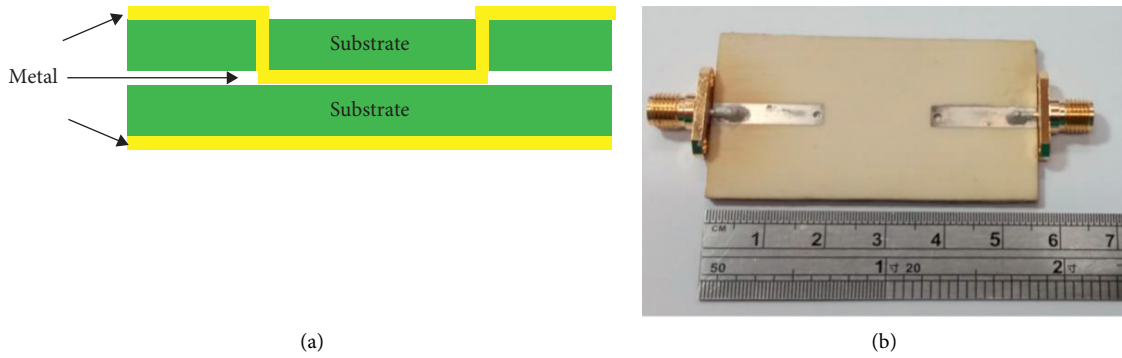
FIGURE 2: (a) The geometry of the fully inkjet-printed microstrip line and (b) the photograph of the test piece.
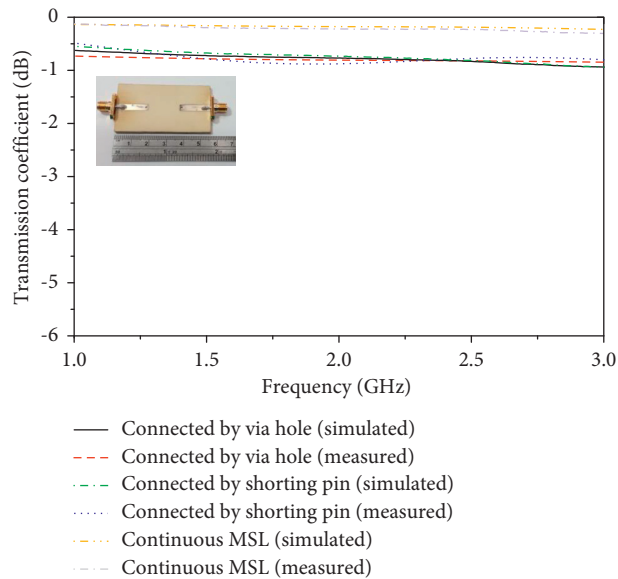

FIGURE 3: Transmission coefficient resulting from microstrip lines connected using the proposed via hole, shorting pin, and intact structure.

transmission coefficients between simulation and measurement; in particular, the difference between the intact trace and the truncated traces is about 0.5 dB. The loss is caused by the discontinuity of two truncated traces. The additional loss of the proposed via hole is similar to that of the shorting pin.

Furthermore, SIWs are constructed by the proposed via hole and shorting pin to compare the insertion loss. The substrate of the SIW is selected as the RO 4003C and PI ($\varepsilon_r = 3.43$ and $\tan\delta = 0.017$), the thickness of which are 0.813 mm and 0.125 mm, respectively. Figure 4 demonstrates the dimensions and photographs of the two-port SIW circuits. The operating frequency is 5.8 GHz. The two ports are terminated with microstrip lines, the characteristic impedance of which is 50 Ω. To reduce the field mismatching, the transition is constructed into a tapered structure. The tapered microstrip line is synthesized using full-wave HFSS simulation, with respect to minimized insertion loss. The distributions of E-fields indicate that the TEM mode is converted into TE_{10} fundamental mode, suggesting that the SIW can propagate waves within the fully inkjet-printed waveguide. Referring to Figure 4(a), the SIWs fabricated on RO 4003C and PI use $A = 60.6$ mm and $B = 1.8$ mm and $A = 50.0$ mm and $B = 0.28$ mm, respectively. To compare the field loss caused by the cylindrical surface via hole and the conventional shorting pin, the SIWs are designed and optimized using both approaches.

Figures 5 and 6 show the simulated and measured results of the SIWs fabricated on RO 4003C and PI, respectively. The discrepancy between simulated and measured results is less than 0.5 dB. Concerning the RO4003 C, the transmission coefficients using the cylindrical-surface via hole and the conventional shorting pin are −1.52 dB and −1.41 dB at 5.8 GHz, respectively, indicating that the via hole can preserve field matching and impedance matching. Concerning the PI, once again, no significant difference is caused by the proposed fabrication. The transmission coefficients using the proposed technique and the conventional shorting pin are −3.88 dB and −4.36 dB, respectively. The insertion loss using the PI is larger than that using the RO 4003C, as the loss tangent is higher and the thickness is smaller. Such additional loss is caused by the material property, instead of the via hole. The results show that the inkjet-printed via hole is capable of preserving SIW signal integrity even though the fabrication procedure is simplified.

3. Fully Inkjet-Printed Wire Bonding

3.1. Proposed Wire Bonding.
Next, the fully inkjet-printing approach is applied to the wire bonding of AiP and SoP. As a proof of concept, Figures 7(a) and 7(c) depict the interconnection using the fully inkjet-printing technology. This scenario does not implement an integrated circuit (IC) die. The interconnection is emulated through two truncated microstrip lines, where the traces are to be connected by a bond wire. The packaging substrate is a 0.813 mm thick RO 4003C. To develop the interconnection between the two traces, the gap is first printed by SU-8 ink ($\varepsilon_r = 3.2$ and $\tan\delta = 0.04$), which can form a dielectric layer [32]. The

thickness of the dielectric layer can be controlled by printing an incremental thickness of 2.5 μm per layer. In this study, four layers of the SU-8 ink are printed and hard-baked at 120°C for 20 minutes. After sintering, the silver nanoparticles are printed onto the SU-8 layer, creating the conductive pathway for each end. The proposed procedure does not require manual placement of a conductive wire, and thus, the continuity of the bond wire is smoother than the conventional approach.

3.2. Validation.
For comparison purposes, another test piece that uses the manual placement of an external copper wire is fabricated, as shown in Figure 7(b). The continuity of the conductive pathway is tested in terms of the relationship between voltage and current. The current is gradually increased from 0.1 A to 0.9 A, and the voltage across the bond wires is measured by a digital multimeter.

Figure 8 presents the results of the two approaches. For the proposed fully inkjet-printing wire bonding, the voltage is varied from 0.26 mV to 2.98 mV. In contrast, for the conventional approach using an external copper wire, the voltage ranges from 0.50 mV to 4.41 mV. The fully inkjet-printing technology leads to smaller resistance, thereby reducing the discontinuity for the interconnection. Moreover, this technique does not require additional manual assembly, and thus, it increases the efficiency in fabrication.

4. Fully Inkjet-Printed Antennas

4.1. SIW Cavity Slot.
After examining the fully inkjet-printed circuits, the proposed technique is applied to antenna applications including SIW cavity antennas and patch antenna arrays. First, we test whether the cavity mode can be generated using the proposed via hole. The RO 4003C and PI described in Section 2 are implemented, and radiation slots are designed within the cavity formed by either shorting pins or inkjet-printed via holes. Figure 9 presents the geometry and photographs of the fully inkjet-printed slot antennas. The cavity is fed by a tapered microstrip line, where the width is optimized with respect to a minimized reflection coefficient at the input port at 5.8 GHz. Referring to Figure 9(a), the optimum geometric parameters for the SIW antennas fabricated on RO 4003C and PI are $a = 7.7$ mm, $b = 30.3$ mm, $c = 16.0$ mm, $d = 3.5$ mm, $e = 12.3$ mm, and $g = 1.8$ mm and $a = 7.8$ mm, $b = 30.2$ mm, $c = 16.1$ mm, $d = 1.2$ mm, $e = 10.2$ mm, and $g = 2.0$ mm, respectively.

The working principle of the SIW cavity slot antenna can be explained by parametric studies. The most crucial parameter is the length of the slot, namely, c. Concerning the PI substrate, c is varied over 15.1 mm, 15.6 mm, 16.1 mm, and 16.6 mm, and the simulated reflection coefficients are shown in Figure 10. The results indicate that variable slot lengths cause significant changes for the resonant frequency. A longer slot length resonates at a lower frequency. To tune the resonant frequency at 5.8 GHz, the length of the slot is selected as $c = 16.1$ mm.

Figure 11 presents the impedance matching for the two antennas fabricated on RO 4003C. At 5.8 GHz, the antennas
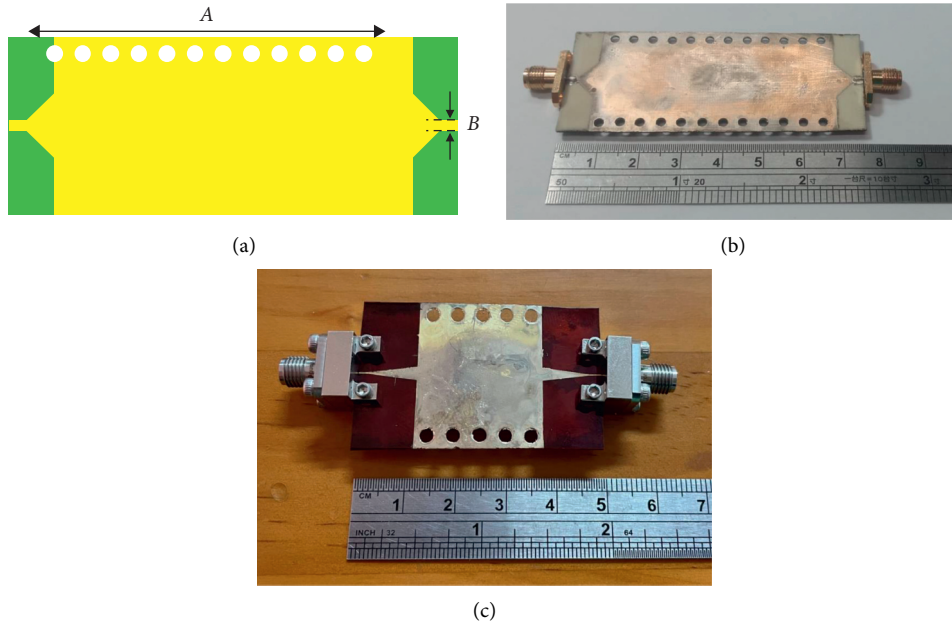
(a)

(b)

(c)

FIGURE 4: (a) The geometry of the fully inkjet-printed SIW and the photographs of the test piece fabricated on (b) RO4003 C and (c) PI.

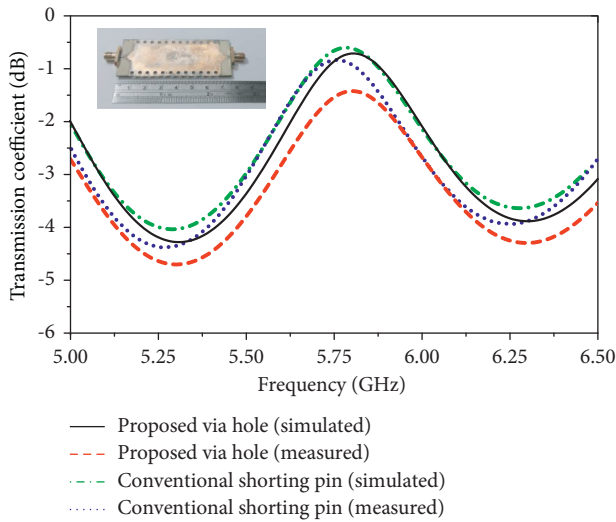Proposed via hole (simulated)
Proposed via hole (measured)
Conventional shorting pin (simulated)
Conventional shorting pin (measured)

FIGURE 5: Transmission coefficient resulting from the via hole and shorting pin fabricated on the RO 4003C substrate.

Proposed via hole (simulated)
Proposed via hole (measured)
Conventional shorting pin (simulated)
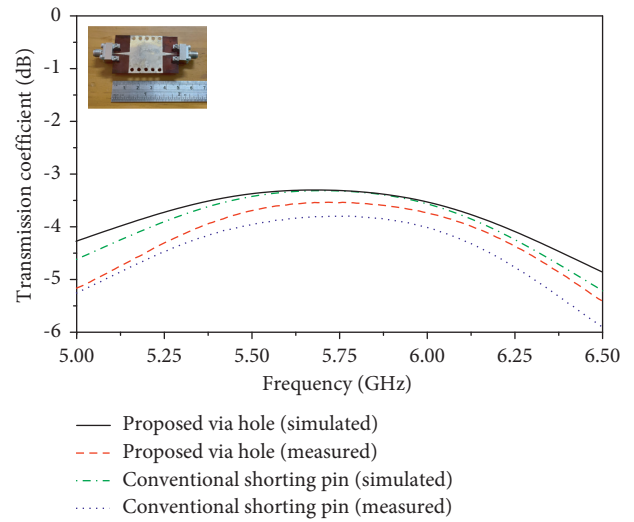Conventional shorting pin (measured)

FIGURE 6: Transmission coefficient resulting from the via hole and shorting pin fabricated on the PI substrate.

demonstrate a reflection coefficient smaller than −15 dB, indicating good impedance matching is achieved using the inkjet-printed cavity. Again, no significant differences are identified between the inkjet-printed via hole and the shorting pin.

Figure 12 demonstrates the radiation patterns of the SIW cavity slots. The patterns indicate broadside radiation with half-power beamwidths (HPBWs) of 72° and 85° on the E-plane and H-plane, respectively, regardless of the type of the substrates. For the SIW cavity formed by the inkjet-printed via hole, the peak gain at 5.8 GHz is 6.1 dBi, which is consistent with the peak gain of the SIW cavity formed by the shorting pin (6.3 dBi). For the antenna fabricated on PI, the gain is reduced due to the additional loss; however, when

the difference between the two fabrication methods is evaluated, the proposed fully inkjet-printed via hole provides similar results. These results confirm that the technique presented in Section 2 can be applied to the development of SIW cavity antennas.

4.2. Flexible Series-Fed Patch Array. Afterward, the fully inkjet-printing technology is extended to flexible antenna arrays. The flexible substrates are selected as PI and polyethylene naphthalate (PEN, $\varepsilon_r = 3.42$ and $\tan\delta = 0.005$), which can conform to nonplanar surface and have been used in a wide range of soft electronics. The thickness of both substrates is 0.125 mm. The capability of the proposed

(a)

(b)

(Unit: mm)

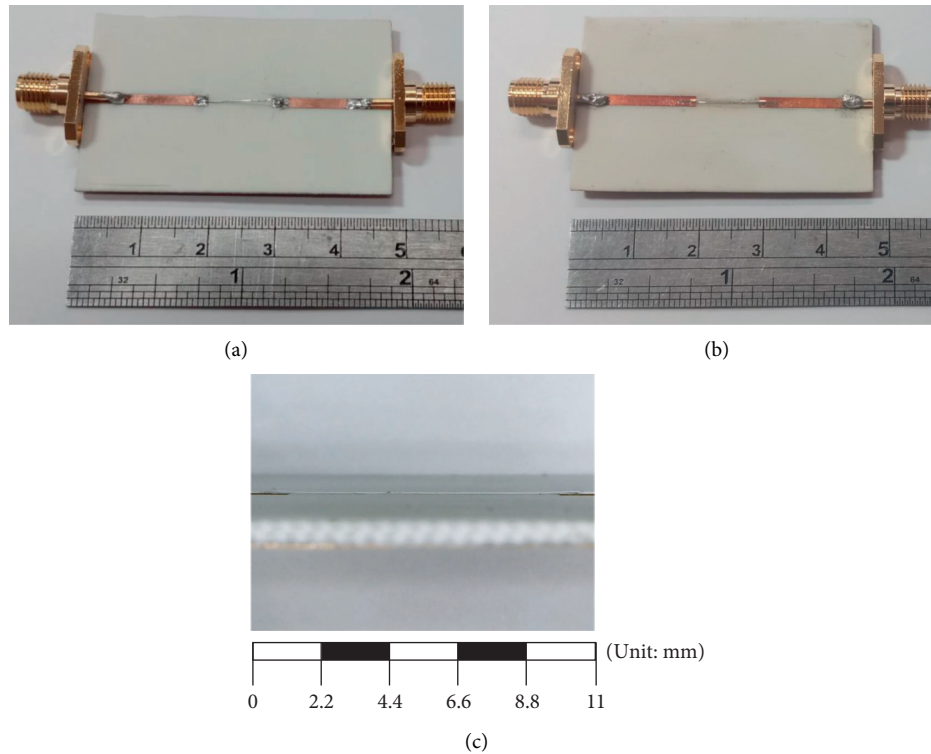|					
0	2.2	4.4	6.6	8.8	11

(c)

FIGURE 7: Interconnected bond wire fabricated using (a) the proposed fully inkjet-printing technique and (b) the conventional approach. (c) The close-up view of the fully inkjet-printed bond wire.
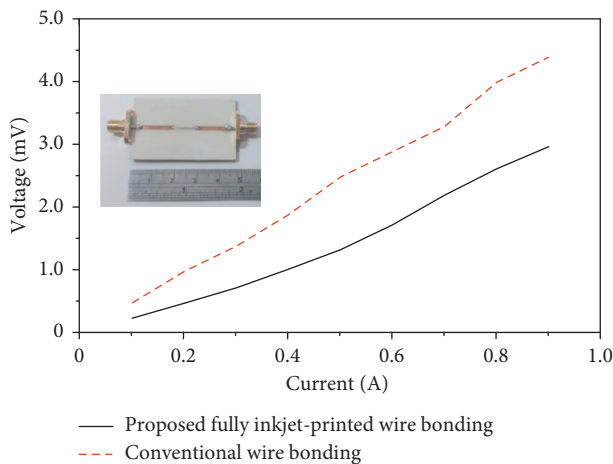

—— Proposed fully inkjet-printed wire bonding
- - - Conventional wire bonding

FIGURE 8: Comparison of the relationship between voltage and current.

method is examined for a series-fed 4×4 patch array. The antenna is designed at 28.0 GHz, and the goal is to cover the millimeter-wave fifth-generation (5G) frequency band.

The design of the 4×4 patch array starts with creating a 4×1 subarray. Figure 13 illustrates the geometry and photographs of the 4×1 subarray. The width of the microstrip line is set to a characteristic impedance of 50 Ω. The dimensions of the patch and the spacing between elements are designed to achieve broadside radiation and sufficient impedance matching. In particular, the spacing

including l_3, l_4, and l_5 are tuned so that the four elements are fed by in-phase currents leading to constructive radiation. Referring to Figure 13(a), the geometric parameters are $l_1 = 9.95$ mm, $l_2 = 2.92$ mm, $l_3 = 2.93$ mm, $l_4 = 2.93$ mm, $l_5 = 2.93$ mm, $l_6 = 2.89$ mm, $w_1 = 0.28$ mm, and $w_2 = 2.91$ mm and $l_1 = 9.85$ mm, $l_2 = 2.87$ mm, $l_3 = 2.89$ mm, $l_4 = 2.89$ mm, $l_5 = 2.89$ mm, $l_6 = 2.84$ mm, $w_1 = 0.27$ mm, and $w_2 = 3.20$ mm for the PI and PEN, respectively.

The working mechanism of the series-fed patch array can be explained by cascading different numbers of patches. Concerning the PI substrate, the design is initiated by creating a single patch element, the dimension of which is 2.92×2.91 mm^2. The reflection coefficient of the single element is shown in Figure 14, illustrating the resonance at 28.0 GHz. To enable in-phase radiation, the second patch element is connected to the initial patch by a separation of half wavelengths, 2.93 mm. The resultant impedance matching is readily achieved, requiring no additional tuning for the geometry, as shown in Figure 14. Following this working mechanism, the third and fourth patch elements are connected to the previous stage. The separation is kept as 2.93 mm to fulfill the requirement of in-phase radiation. The antenna performance is also depicted in Figure 14. As a result, the 4×1 subarray is designed in a systematic manner.

After examining the circuit and radiation parameters for the subarray, a four-way power divider is designed to feed each subarray. Figure 15 shows the geometry and photographs of the 4×4 array. The geometric parameters of the elements require further fine-tuning to accommodate various folding angles. Referring to Figure 15(a), the geometric
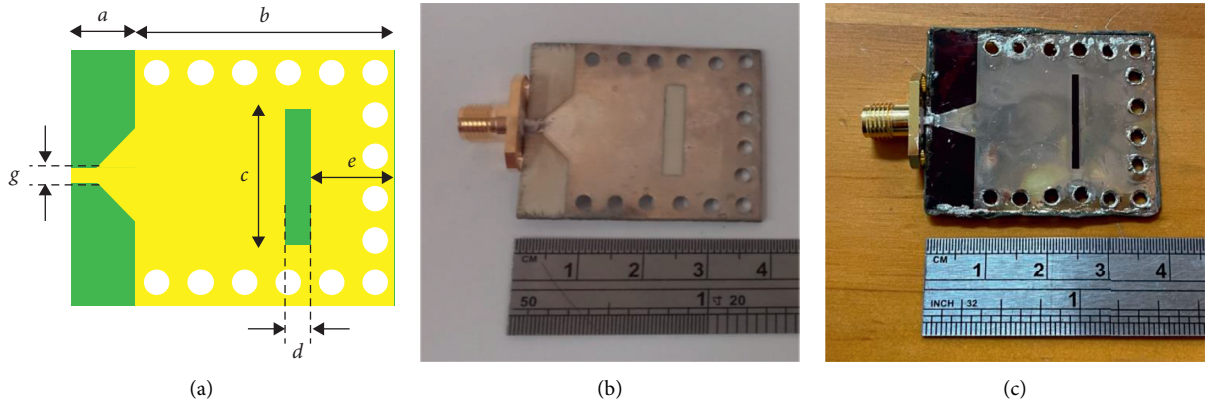
(a) (b) (c)

FIGURE 9: (a) The geometry of the fully inkjet-printed SIW antenna and the photographs of the SIW antenna fabricated on (b) RO4003 C and (c) PI.
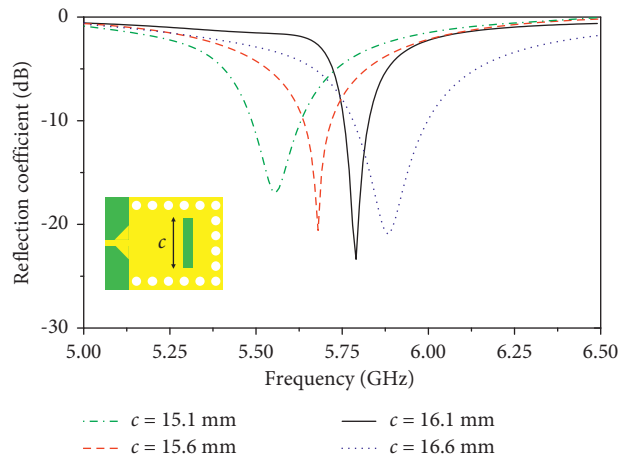

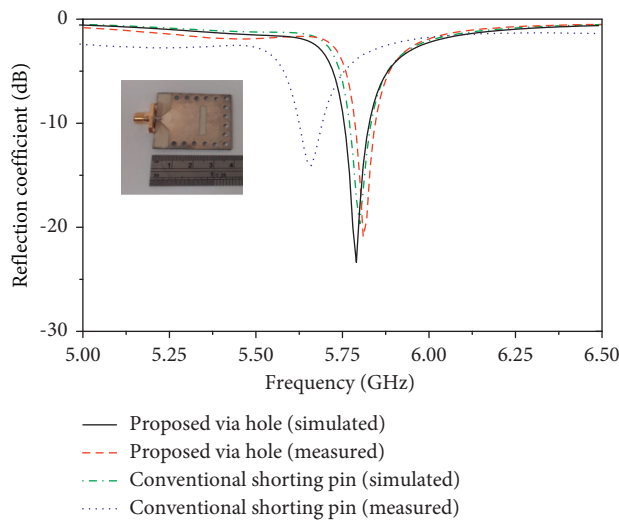FIGURE 10: Parametric study for the length of the SIW cavity slot antenna.

FIGURE 11: Reflection coefficient of the SIW cavity slot antennas fabricated using the proposed fully inkjet-printed via hole and the shorting pin.
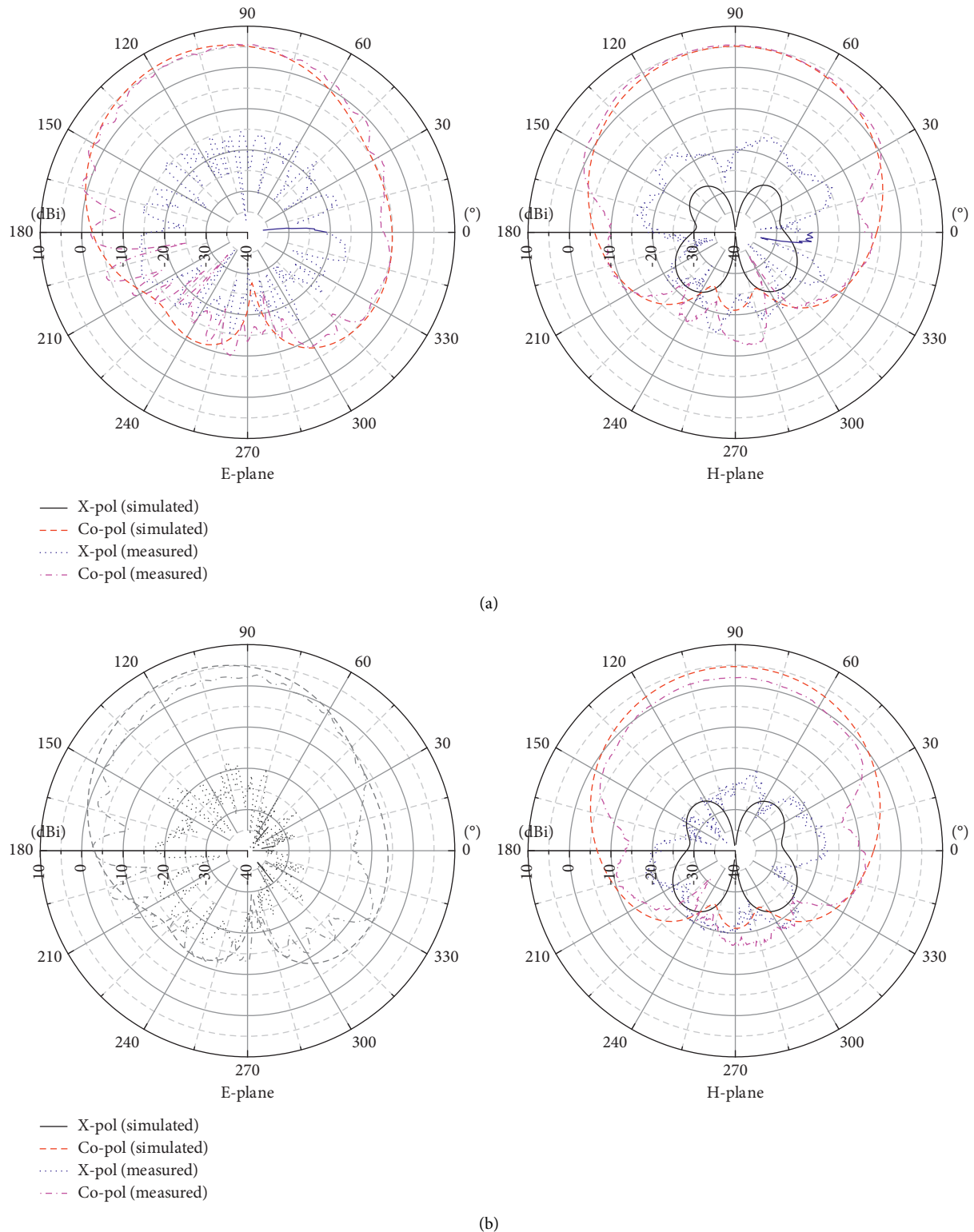
(a)

(b)

FIGURE 12: Pattern of the SIW cavity slot antennas fabricated on (a) RO 4003C and (b) PI.

parameters are $L_1 = 6.78$ mm, $L_2 = 0.06$ mm, $L_3 = 0.96$ mm, $L_4 = 0.97$ mm, $L_5 = 0.06$ mm, $L_6 = 1.70$ mm, $L_7 = 1.66$ mm, $L_8 = 2.92$ mm, $L_9 = 2.93$ mm, $L_{10} = 2.99$ mm, $L_{11} = 2.94$ mm, $L_{12} = 2.80$ mm, $W_1 = 0.28$ mm, $W_2 = 7.03$ mm, $W_3 = 0.15$ mm, $W_4 = 0.28$ mm, $W_5 = 3.51$ mm,

$W_6 = 0.15$ mm, $W_7 = 0.28$ mm, and $W_8 = 2.91$ mm and $L_1 = 6.69$ mm, $L_2 = 0.06$ mm, $L_3 = 0.95$ mm, $L_4 = 0.98$ mm, $L_5 = 0.06$ mm, $L_6 = 1.68$ mm, $L_7 = 1.64$ mm, $L_8 = 2.87$ mm, $L_9 = 2.89$ mm, $L_{10} = 2.89$ mm, $L_{11} = 2.89$ mm, $L_{12} = 2.78$ mm, $W_1 = 0.27$ mm, $W_2 = 6.96$ mm, $W_3 = 0.14$ mm,
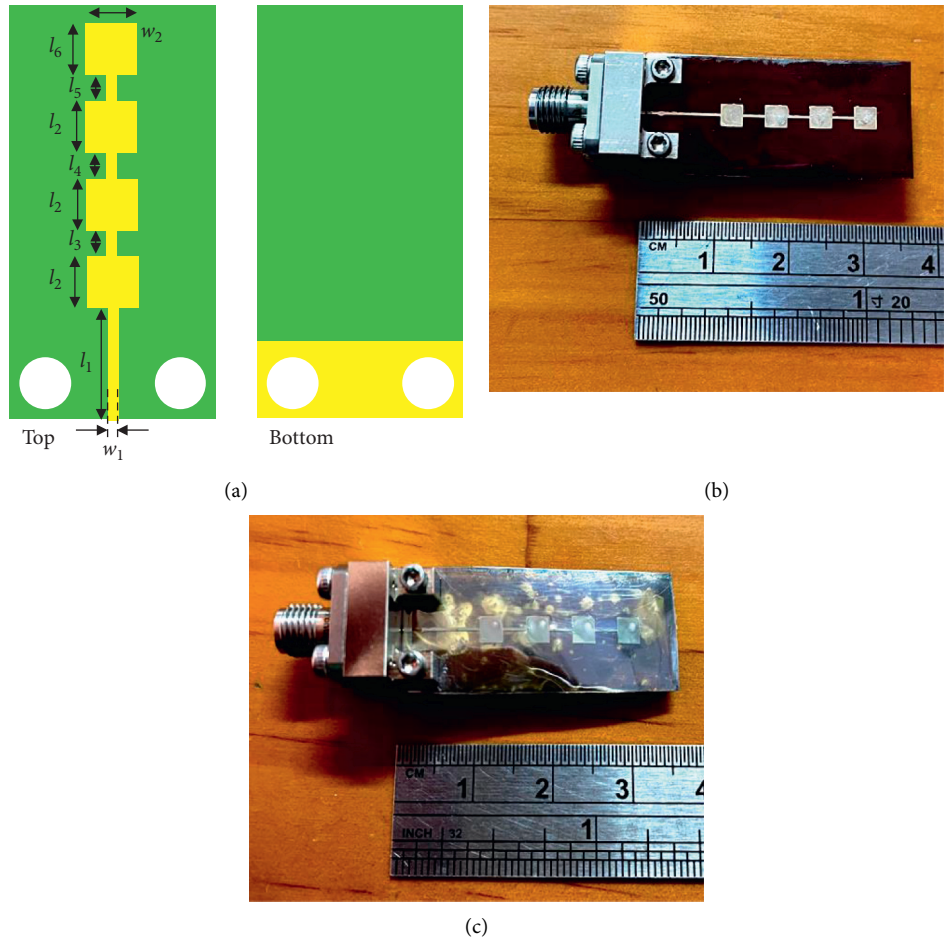
(a)

(b)

(c)

FIGURE 13: (a) The geometry of the fully inkjet-printed 4×1 flexible subarray and the photographs of the antenna fabricated on (b) PI and (c) PEN.
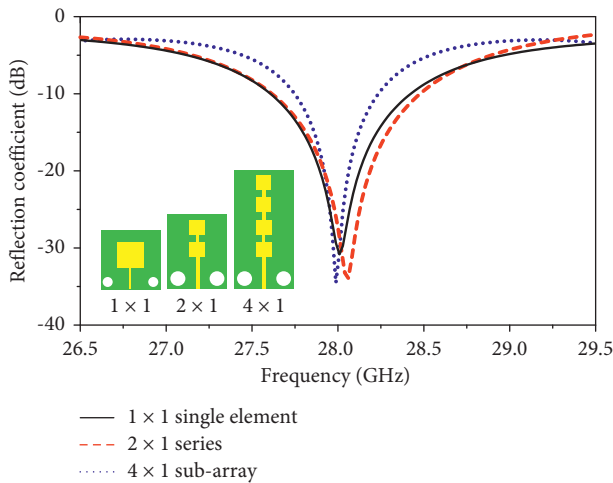

FIGURE 14: Working mechanism of the series-fed patch array.

$W_4 = 0.27$ mm, $W_5 = 3.48$ mm, $W_6 = 0.14$ mm, $W_7 = 0.27$ mm, and $W_8 = 3.20$ mm for the PI and PEN, respectively.

These subarrays and 4×4 arrays are tested in terms of different folding angles. Figure 16 illustrates the folding

condition for these antennas. The folding of the substrate is characterized by placing the antenna on curved foam surfaces. The foam cylinders have different radii, mimicking various folding angles. The antenna performance is tested in planar mode and under bending. The folding angles are selected as 20°, 30°, and 40°, corresponding with radii of 21.5 mm, 14.3 mm, and 10.7 mm, respectively.

Figure 17 presents the impedance matching of the subarray and the 4×4 array against folding extents. The subarray depicts robust impedance matching except for a folding angle of 40°. Under the planar mode and slight bending, the impedance bandwidths are consistent and can cover the millimeter-wave 5G frequency band. Concerning the 4×4 array, the impedance bandwidth is broadened and less sensitive to the effect of folding. The underlying reason is the length of the short side. For the 4×1 subarray, the length of the short side is 15 mm, whereas the 4×4 array has a short side of 30 mm. Thus, the phase center of the 4×1 subarray is closer to the edge of the short side; when the antenna is folded by a larger angle, such as 40° in this case, the central element is directly bent, and thus, the geometry suffers from more severe deformation, which causes a frequency shift for the reflection coefficient. As the 4×4 array uses a wider short side (30 mm), the phase center is away from the edge, and
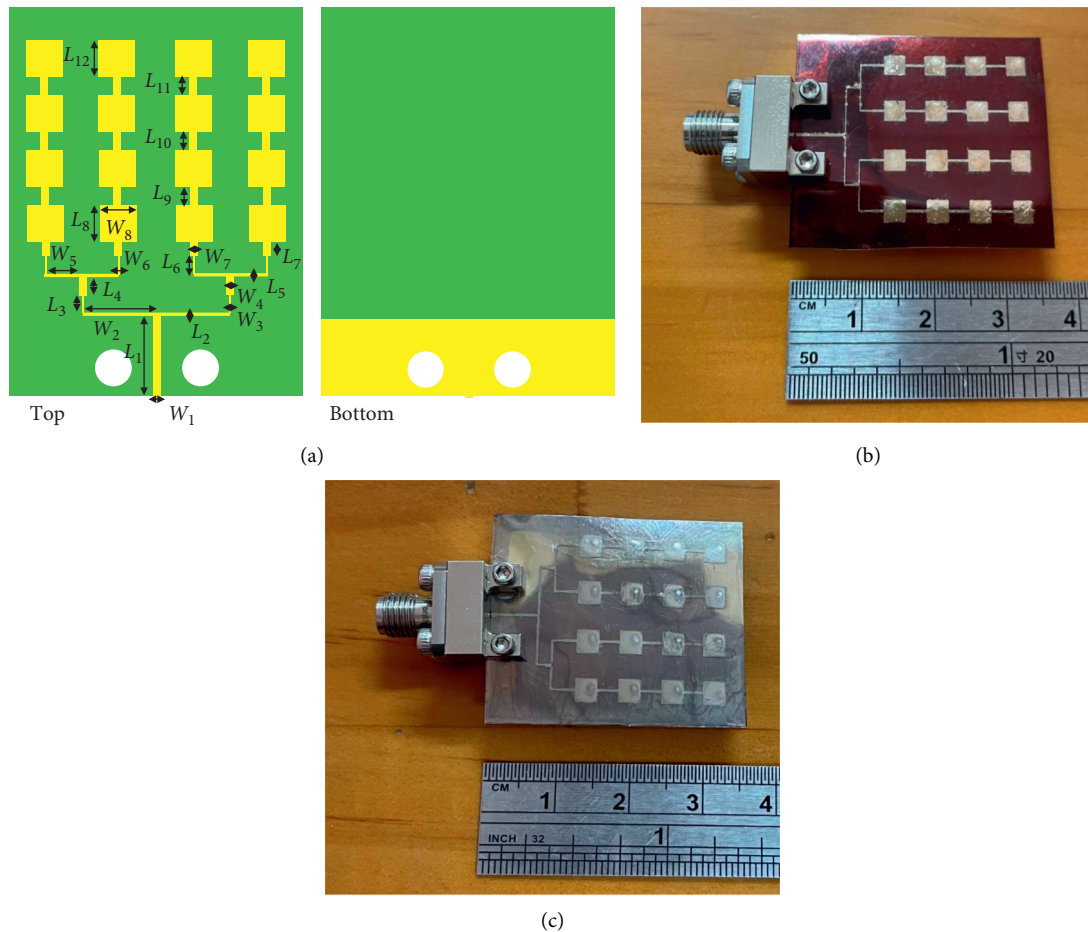
FIGURE 15: (a) The geometry of the fully inkjet-printed 4 × 4 flexible patch array and the photographs of the antenna fabricated on (b) PI and (c) PEN.
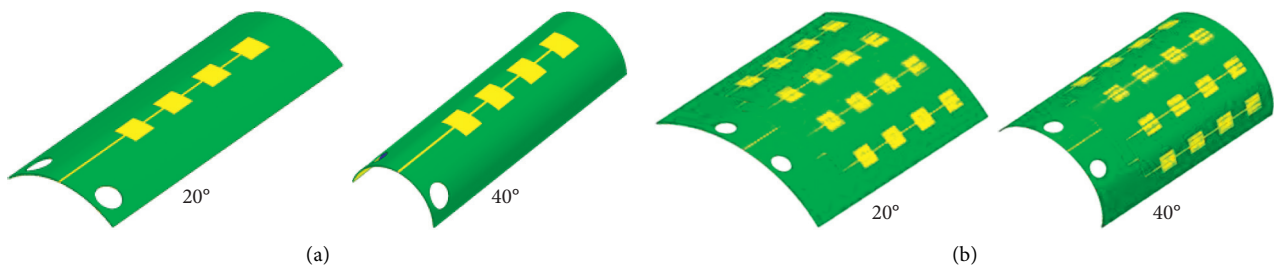

FIGURE 16: Illustrations of the folding of (a) 4 × 1 subarray and (b) 4 × 4 patch array.

the central element is slightly deformed. This keeps the impedance matching robust against the folding angles. Nevertheless, the reflection coefficients are below –10 dB and over 27.5–28.5 GHz for all the scenarios.

Next, the antennas are tested with respect to far-field radiation. Figure 18 shows the experiment in a far-field anechoic chamber. Figure 19 shows the radiation patterns. For the subarray, the HPBWs on the E-plane are 21°, 22°, and 23° for folding angles of 0°, 20°, and 40°, respectively, whereas the HPBWs on the H-plane are 69°, 74°, and 84°. Thus, a larger folding extent broadens the HPBW. Nevertheless, significant broadside radiation is observed, and the

broadside gains at folding angles of 0°, 20°, and 40° are 10.1 dBi, 9.9 dBi, and 9.2 dBi, respectively. For the 4 × 4 array, the HPBWs on the E-plane (H-plane) are 23° (18°), 24° (26°), and 25° (75°) for folding angles of 0°, 20°, and 40°, respectively. Once again, the larger the folding angle, the broader the HPBW is. The E-plane pattern shows a more directive main beam as compared to the H-plane pattern. As illustrated in Figure 16, the folding is performed along the direction of the H-field. The E-plane pattern is created by the four elements connected in series, so they are not affected by various folding angles. In contrast, as the antenna structure is folded along the direction of the H-field, the elements on the fringe
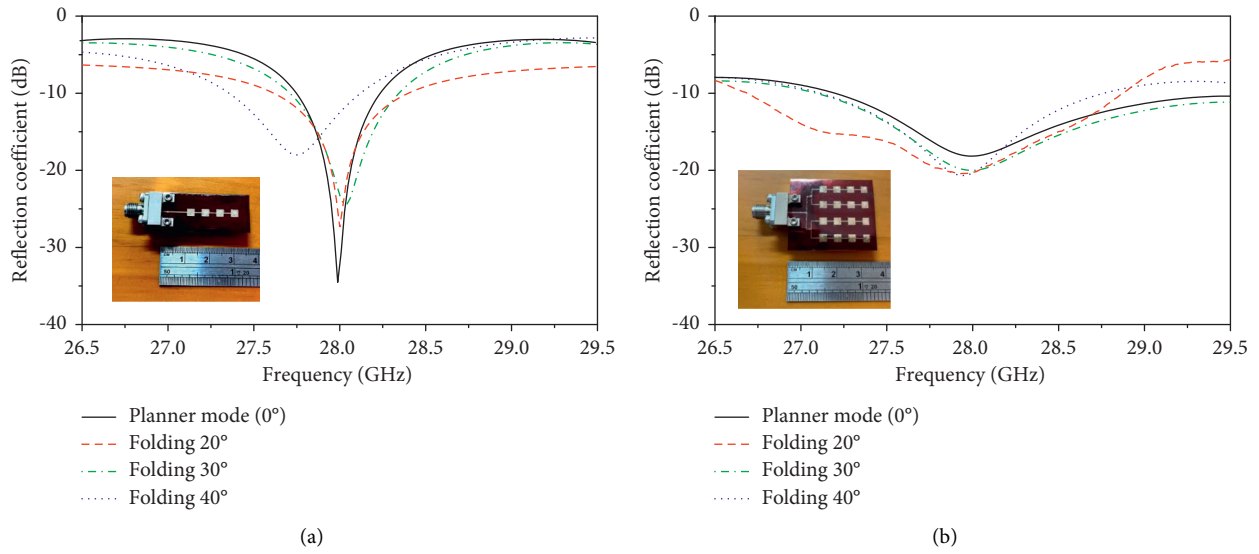
(a)

(b)

Figure 17: Reflection coefficient of the (a) 4×1 subarray and (b) 4×4 patch array under different folding angles.
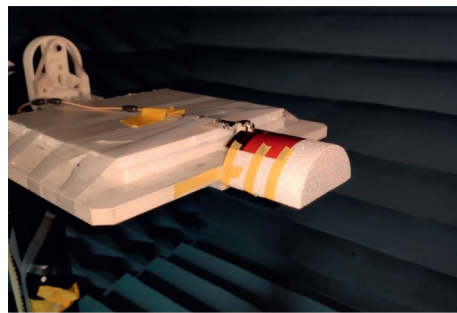

Figure 18: Photograph of the folding of the antenna under test for far-field measurement.
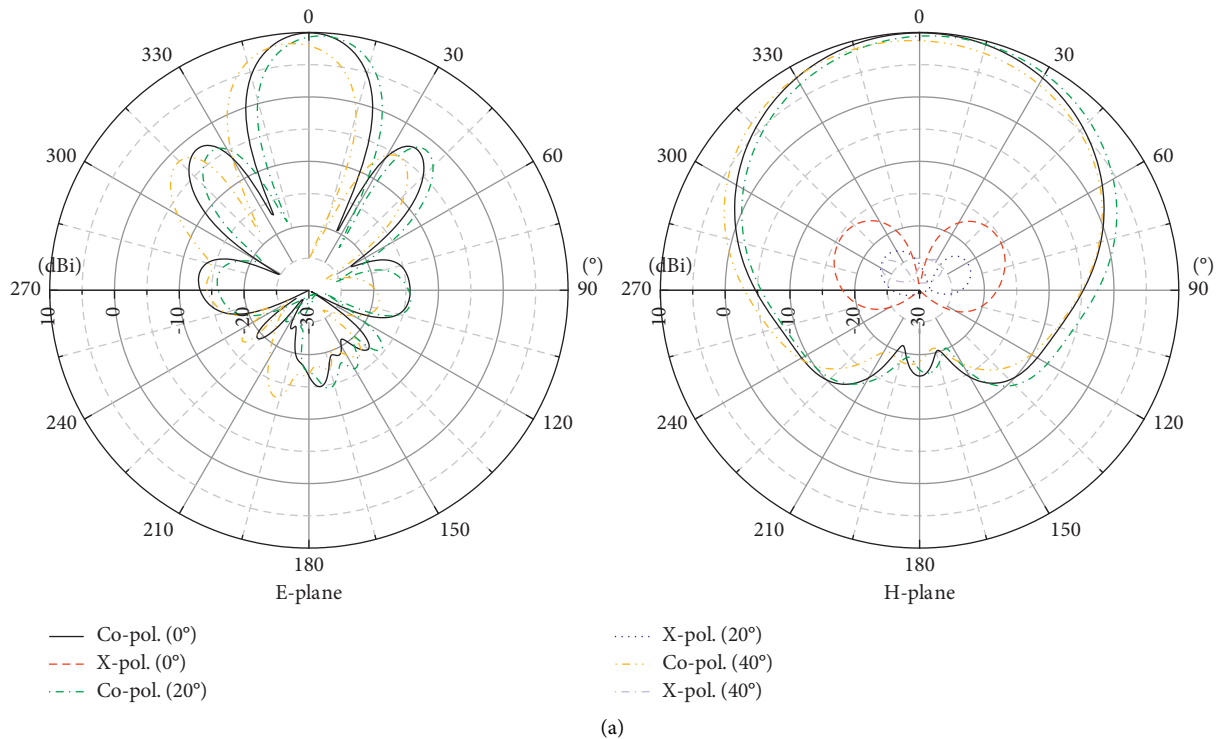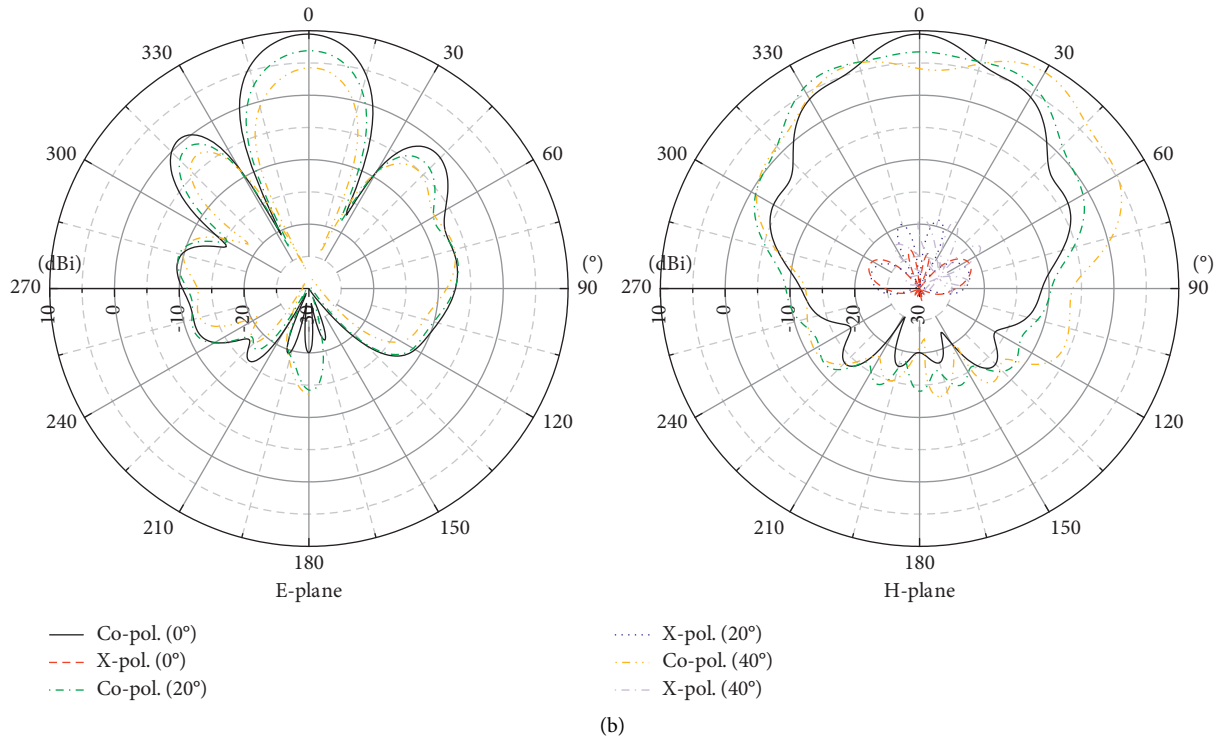

(a)

Figure 19: Continued.

Figure 19: Patterns of the (a) 4×1 subarray and (b) 4×4 patch array under different folding angles.

fail to create in-phase radiation with the elements located on the phase center. This broadens the main beam of the H-plane plane and reduces the directional property. This suggests that the folding angle of the flexible array applications should not exceed $20°$.

In addition, the gain and efficiency results as the function of frequency are shown in Figure 20. The realized gain agrees with the patterns depicted in Figure 19. When the 4×4 patch array is folded as severely as $40°$, the increasing HPBW reduces the directivity of the antenna. This further lowers the peak gain. Additionally, the radiation efficiency is reduced over folded angles. This confirms the observation of the fringing elements that have difficulty creating in-phase radiation with the central elements.

5. Discussion

The distinct features of the proposed technique are shown in Table 1. As can be seen, this study advances the inkjet-printing technology to the fully inkjet-printed RF front end. Some studies employ inkjet printing for the metallization of passive components, whereas the vias are fabricated by copper pillars or other conductive pins [3]– [6, 28, 29]. This additional procedure is not compatible with inkjet printing. Moreover, the silver nanoparticles and the copper rivets require additional soldering to ensure conductive continuity, thereby decreasing the efficiency of manufacturing.
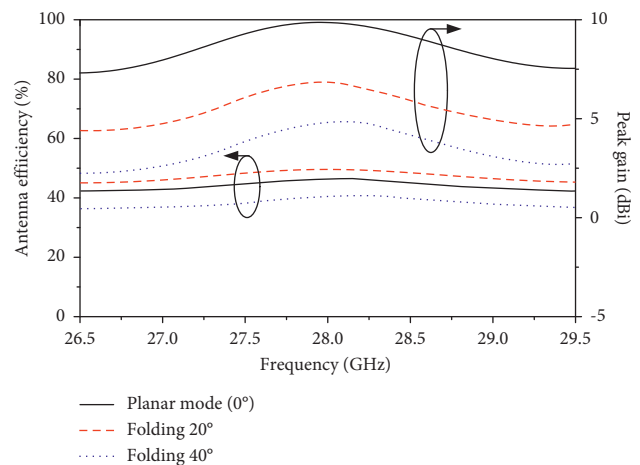
Figure 20: Antenna efficiency and realized peak gain of the 4×4 patch array under different folding angles.

Although some studies have employed fully inkjet-printed vias to develop SIW antennas [30, 31], this study reduces the misalignment mismatch, mechanical stress, and fabrication complexity from the laser-drilled and multiple concentric stepped-via topology. In addition, the proposed technique can be applied to the wire bonding for active components [32]. Summarizing these features, the contribution of this study is the efficiency enhancement of inkjet-

TABLE 1: Distinct features of the proposed technique.

Reference	Fabrication of vias	Fabrication of wire bonding	Integration of fully inkjet-printed vias and an antenna
[3]	Copper microvias	N/A	No
[4]	Thin copper wire	N/A	No
[5]	Thin wire	N/A	No
[6]	Conductive epoxy	N/A	No
[28]	Copper pillars	N/A	No
[29]	Conductive epoxy	Conductive epoxy	No
[30]	Inkjet printing	N/A	Yes
[31]	Inkjet printing	N/A	No
[32]	N/A	Inkjet printing	No
This study	Inkjet printing	Inkjet printing	Yes

printing fabrication and the continuous improvement of conductive pathways.

6. Conclusion

The fully inkjet-printing technology with reduced fabrication complexity has been reported. The proposed technique is demonstrated through three components, namely, via holes, wire bonding, and flexible antenna arrays. The novelty of the proposed technique is fourfold. First, the proposed fully inkjet-printing technology integrates the fabrication of the entire RF front end, including antennas, passive components, via holes, and wire bonding for active components, using only one metallization procedure. Second, as compared to the earlier inkjet-printed via holes, the proposed manufacturing method prevents the requirement of alignment sensitivity or the precise control of laser power level. Third, concerning the fully inkjet-printed wire bonding, the proposed technique is compatible with other inkjet-printed components, greatly reducing the discontinuity caused by the conventional external wire. The proposed technique has been compared with the conventional PCB fabrication. The results suggest that the fully inkjet-printing technology leads to superior performance, whereas the fabrication complexity and manufacturing cost are reduced. Fourth, the fully inkjet-printing technology can generate SIW cavity antennas with desirable reflection coefficients and radiation patterns, and it can develop patch antenna arrays with strong broadside radiation against moderate folding of the substrate. It is expected that the proposed technique enhances the efficiency of fabrication in cost and time, bringing more fascinating inkjet-printed AiP, SIW, and SoP applications.

Data Availability

The simulated and measured data used to support the findings of this study are included within the article.

Conflicts of Interest

The authors declare that they have no conflicts of interest.

Acknowledgments

References

[1] N. Guo and M. C. Leu, "Additive manufacturing: technology, applications and research needs," *Frontiers of Mechanical Engineering*, vol. 8, no. 3, pp. 215–243, 2013.

[2] B. Ghassemiparvin and N. Ghalichechian, "Design, fabrication, and testing of a helical antenna using 3D printing technology," *Microwave and Optical Technology Letters*, vol. 62, no. 4, pp. 1577–1580, 2020.

[3] T.-H. Lin, K. Kanno, A. O. Watanabe et al., "Broadband and miniaturized antenna-in-package (AiP) design for 5G applications," *IEEE Antennas and Wireless Propagation Letters*, vol. 19, no. 11, pp. 1963–1967, 2020.

[4] R. Moro, M. Bozzi, S. Kim, and M. Tentzeris, "Novel inkjet-printed substrate integrated waveguide (SIW) structures on low-cost materials for wearable applications," in *Proceedings of the 2012 42nd European Microwave Conference*, pp. 72–75, Amsterdam, Netherlands, October 2012.

[5] A. Izzuddin, A. Dewantari, E. Setijadi, E. Palantei, E. T. Rahardjo, and A. Munir, "Design of 2.4 GHz slotted SIW array antenna for WLAN application," in *Proceedings of the International Conference on Radar, Antenna, Microwave, Electronics, and Telecommunications (ICRAMET)*, pp. 70–73, Tangerang, Indonesia, November 2020.

[6] S. Kim, H. Aubert, and M. Tentzeris, "An inkjet-printed flexible broadband coupler in substrate integrated waveguide (SIW) technology for sensing, RFID and communication applications," in *Proceedings of the IIEEE MTT-S Int Microwave Symp (IMS2014)*, pp. 1–4, Tampa, Florida, USA, June 2014.

[7] J. G. Hester, S. Kim, J. Bito et al., "Additively manufactured nanotechnology and origami-enabled flexible microwave electronics," *Proceedings of the IEEE*, vol. 103, no. 4, pp. 583–606, 2015.

[8] P. M. Njogu, B. Sanz-Izquierdo, S. Y. Jun et al., "Evaluation of planar inkjet-printed antennas on a low-cost origami flapping robot," *IEEE Access*, vol. 8, pp. 164103–164113, 2020.

[9] S. Y. Jun, A. Shastri, B. Sanz-Izquierdo, D. Bird, and A. McClelland, "Investigation of antennas integrated into disposable unmanned aerial vehicles," *IEEE Transactions on Vehicular Technology*, vol. 68, no. 1, pp. 604–612, 2019.

[10] S. I. H. Shah, M. M. Tentzeris, and S. Lim, "Low-cost circularly polarized origami antenna," *IEEE Antennas and Wireless Propagation Letters*, vol. 16, pp. 2026–2029, 2017.

[11] S. I. H. Shah, D. Lee, M. M. Tentzeris, and S. Lim, "A novel high-gain tetrahedron origami," *IEEE Antennas and Wireless Propagation Letters*, vol. 16, pp. 848–851, 2017.

[12] X. Guo, Y. Hang, Z. Xie, C. Wu, L. Gao, and C. Liu, "Flexible and wearable 2.45 GHz CPW-fed antenna using inkjet-

printing of silver nanoparticles on pet substrate," *Microwave and Optical Technology Letters*, vol. 59, no. 1, pp. 204–208, 2017.

[13] K. Hettak, A. Petosa, and R. James, "Flexible polyethylene terephthalate-based inkjet printed CPW-fed monopole antenna for 60 GHz ISM applications," in *Proceedings of the 2014 IEEE Antennas and Propagation Society International Symposium (APSURSI)*, pp. 1447–1450, Memphis, Tennessee, USA, July 2013.

[14] J. Pourahmadazar and T. A. Denidni, "Millimeter-wave planar antenna on flexible polyethylene terephthalate substrate with water base silver nanoparticles conductive ink," *Microwave and Optical Technology Letters*, vol. 60, no. 4, pp. 887–891, 2018.

[15] O. M. Sanusi, F. A. Ghaffar, A. Shamim, M. Vaseem, Y. Wang, and L. Roy, "Development of a 2.45 GHz antenna for flexible compact radiation dosimeter tags," *IEEE Transactions on Antennas and Propagation*, vol. 67, no. 8, pp. 5063–5072, 2019.

[16] V. K. Palukuru, A. Pekonen, V. Pynttäri, R. Mäkinen, J. Hagberg, and H. Jantunen, "An inkjet-printed inverted-F antenna for 2.4-GHz wrist applications," *Microwave and Optical Technology Letters*, vol. 51, no. 12, pp. 2936–2938, 2009.

[17] H. R. Khaleel, "Design and fabrication of compact inkjet printed antennas for integration within flexible and wearable electronics," *IEEE Transactions on Components, Packaging, and Manufacturing Technology*, vol. 4, no. 10, pp. 1722–1728, 2014.

[18] B. S. Cook, B. Tehrani, J. R. Cooper, and M. M. Tentzeris, "Multilayer inkjet printing of millimeter-wave proximity-fed patch arrays on flexible substrates," *IEEE Antennas and Wireless Propagation Letters*, vol. 12, pp. 1351–1354, 2013.

[19] T. Lin, R. Bahr, M. M. Tentzeris, P. M. Raj, V. Sundaram, and R. Tummala, "Novel 3D-/inkjet-printed flexible on-package antennas, packaging structures, and modules for broadband 5G applications," in *Proceedings of the Proc IEEE 68th Electron Compon Technol Conf*, pp. 214–220, San Diego, California, May 2018.

[20] M. A. H. Khan, S. Ali, J. Bae, and C. H. Lee, "Inkjet printed transparent and bendable patch antenna based on polydimethylsiloxane and indium tin oxide nanoparticles," *Microwave and Optical Technology Letters*, vol. 58, no. 12, pp. 2884–2887, 2016.

[21] W. Su, J. Zhu, H. Liao, and M. M. Tentzeris, "Wearable antennas for cross-body communication and human activity recognition," *IEEE Access*, vol. 8, pp. 58575–58584, 2020.

[22] M. F. Farooqui and A. Shamim, "Dual band inkjet printed bow-tie slot antenna on leather," in *Proceedings of the 7th Eur Conf Antennas Propag.*, pp. 3287–3290, Gothenburg, Sweden, April 2013.

[23] I. Llatser, C. Kremers, A. Cabellos-Aparicio, J. M. Jornet, E. Alarcón, and D. N. Chigrin, "Graphene-based nano-patch antenna for terahertz radiation," *Photonics and Nanostructures - Fundamentals and Applications*, vol. 10, no. 4, pp. 353–358, 2012.

[24] S. Genovesi, F. Costa, F. Fanciulli, and A. Monorchio, "Wearable inkjet-printed wideband antenna by using miniaturized AMC for sub-GHz applications," *IEEE Antennas and Wireless Propagation Letters*, vol. 15, pp. 1927–1930, 2016.

[25] A. Sharif, J. Ouyang, F. Yang et al., "Low-cost inkjet-printed UHF RFID tag-based system for internet of things applications using characteristic modes," *IEEE Internet of Things Journal*, vol. 6, no. 2, pp. 3962–3975, 2019.

[26] M. M. Khan, F. A. Tahir, M. F. Farooqui, A. Shamim, and H. M. Cheema, "3.56 bits/cm2 compact inkjet printed and application-specific chipless RFID tag," *IEEE Antennas and Wireless Propagation Letters*, vol. 15, pp. 1109–1112, 2015.

[27] M. Borgese, F. A. Dicandia, F. Costa, S. Genovesi, and G. Manara, "An inkjet printed chipless RFID sensor for wireless humidity monitoring," *IEEE Sensors Journal*, vol. 17, no. 15, pp. 4699–4707, 2017.

[28] R. Moro, S. Kim, M. Bozzi, and M. Tentzeris, "Inkjet-printed paper-based substrate-integrated waveguide (SIW) components and antennas," *International Journal of Microwave and Wireless Technologies*, vol. 5, no. 3, pp. 197–204, 2013.

[29] A. Rida, R. Vyas, L. Yang, C. Kruesi, and M. M. Tentzeris, "'Low cost inkjet-printing paper-based modules for RFID sensing and wireless applications," in *Proceedings of the Eur. Microw. Conf. (EuMW)*, pp. 1715–1718, Amsterdam, The Netherlands, October 2008.

[30] S. Kim, A. Shamim, A. Georgiadis, H. Aubert, and M. M. Tentzeris, "Fabrication of fully inkjet-printed vias and SIW structures on thick polymer substrates," *IEEE Transactions on Components, Packaging, and Manufacturing Technology*, vol. 6, no. 3, pp. 486–496, 2016.

[31] I. Reinhold, M. Thielen, W. Voit, W. Zapka, R. Gotzen, and H. Bohlmann, "Inkjet printing of electrical vias," in *Proceedings of the 18th Eur Microelectron Packag Conf.*, pp. 1–4, Brighton, 2011.

[32] B. K. Tehrani, B. S. Cook, and M. M. Tentzeris, "Inkjet-printed 3d interconnects for millimeter-wave system-on-package solutions," in *Proceedings of the 2016 MTT-S International Microwave Symposium*, pp. 1–4, San Francisco, California, USA, 2016.

[33] R. Vashi, T. Upadhyaya, and A. Desai, "Graphene-based wide band semi-flexible array antenna with parasitic patch for smart wireless devices," *International Journal of Microwave and Wireless Technologies*, vol. 14, no. 1, pp. 86–94, 2022.

[34] H. Subbaraman, D. T. Pham, X. Xu et al., "Inkjet-printed two-dimensional phased-array antenna on a flexible substrate," *IEEE Antennas and Wireless Propagation Letters*, vol. 12, pp. 170–173, 2013.

[35] A. T. Castro and S. K. Sharma, "Inkjet-printed wideband circularly polarized microstrip patch array antenna on a PET film flexible substrate material," *IEEE Antennas and Wireless Propagation Letters*, vol. 17, no. 1, pp. 176–179, Jan. 2018.